

1  
2  
3  
4  
5  
6  
7  
8  
9  
10  
11  
12  
13  
14  
15  
16  
17  
18  
19

*Geophysical Research Letters*

Supporting Information for

**First assessment of cloud-land coupling in LASSO Large-Eddy Simulations**

Haipeng Zhang<sup>1,2</sup>, Tianning Su<sup>1,2,3</sup>, Youtong Zheng<sup>4,5</sup>, and Zhanqing Li<sup>1,2</sup>

<sup>1</sup>Department of Atmospheric and Oceanic Science, University of Maryland, College Park, MD, USA

<sup>2</sup>Earth System Science Interdisciplinary Center, University of Maryland, College Park, MD, USA

<sup>3</sup>Lawrence Livermore National Laboratory, Livermore, CA, USA

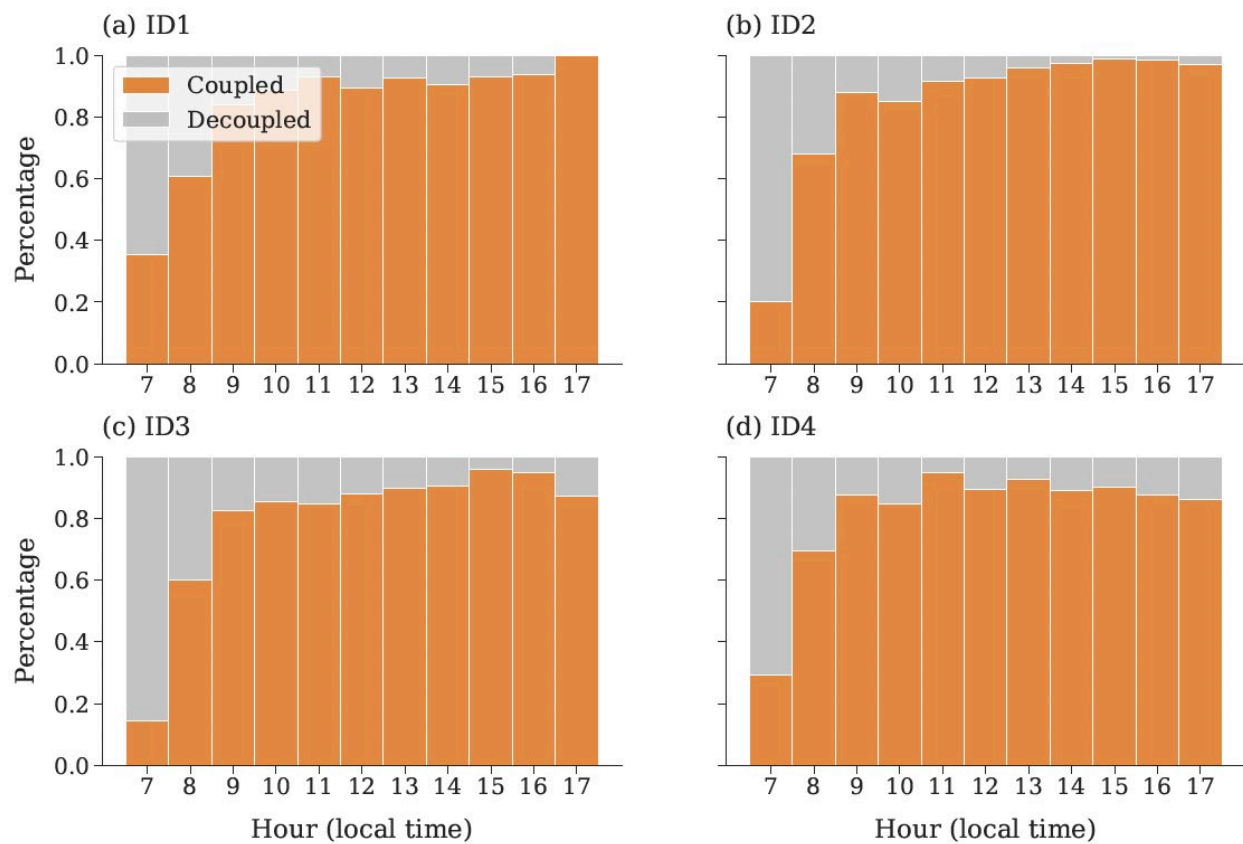
<sup>4</sup>Department of Atmospheric and Earth Science, University of Houston, Houston, TX, USA

<sup>5</sup>Institute of Climate and Atmospheric Science, University of Houston, Houston, TX, USA

**Contents of this file**

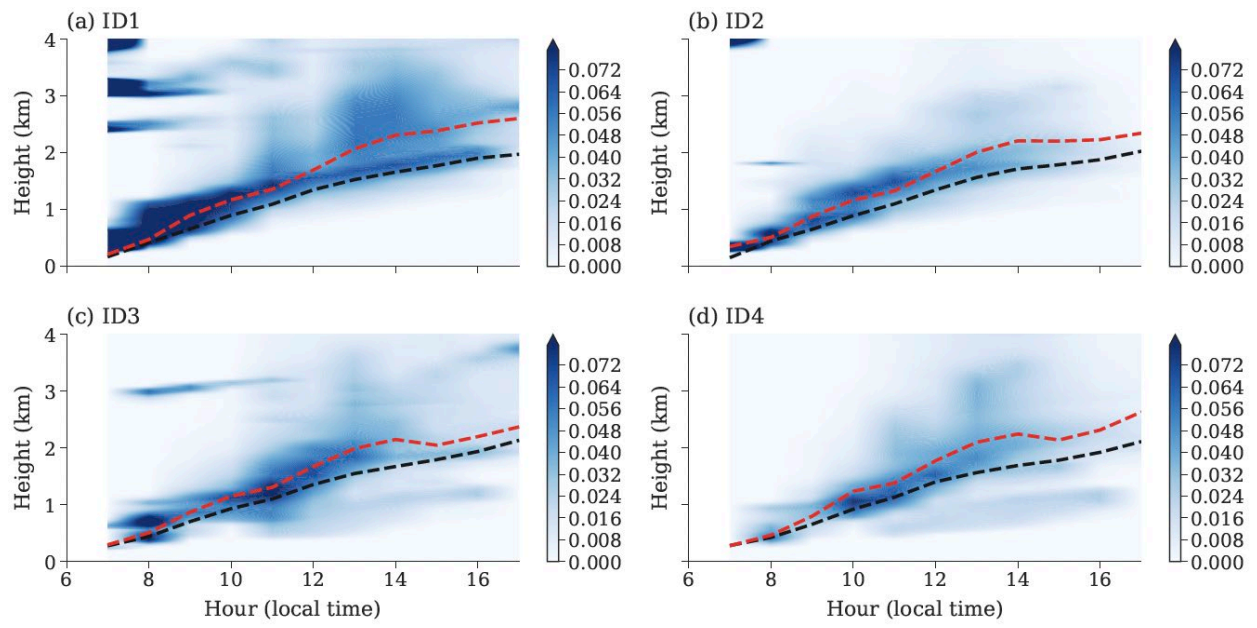
Figures S1 to S8

20 **Figures:**  
21  
22  
23



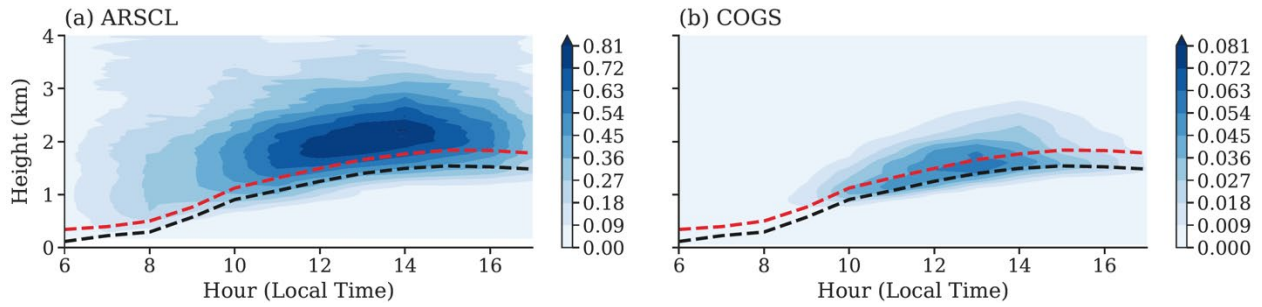
24  
25  
26  
27  
28  
29  
30  
31  
32  
33

**Figure S1.** Same as Figure 1c but for simulation sets labeled as ID 1, 2, 3, and 4.



34  
 35  
 36  
 37  
 38  
 39  
 40  
 41  
 42

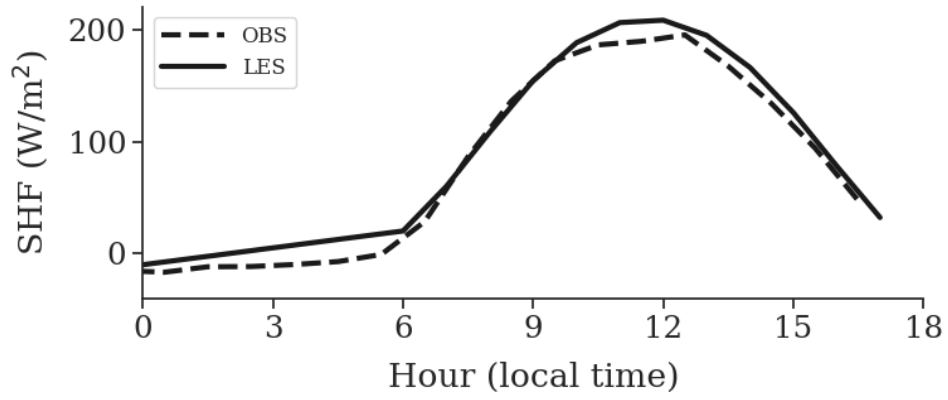
**Figure S2.** Same as Figure 2b but for simulation sets labeled as ID 1, 2, 3, and 4.



43  
 44  
 45  
 46  
 47  
 48  
 49  
 50  
 51  
 52  
 53  
 54  
 55  
 56

**Figure S3.** Time-height cross sections of cloud fraction averaged for the case days from 2018 to 2019 (including all types of clouds) from the (a) ARM Active Remote Sensing of Clouds (ARSCL) and (b) Clouds Optically Gridded by Stereo (COGS) products. The red and black dashed lines represent the lidar-derived boundary-layer height and the lifted condensation level, respectively.

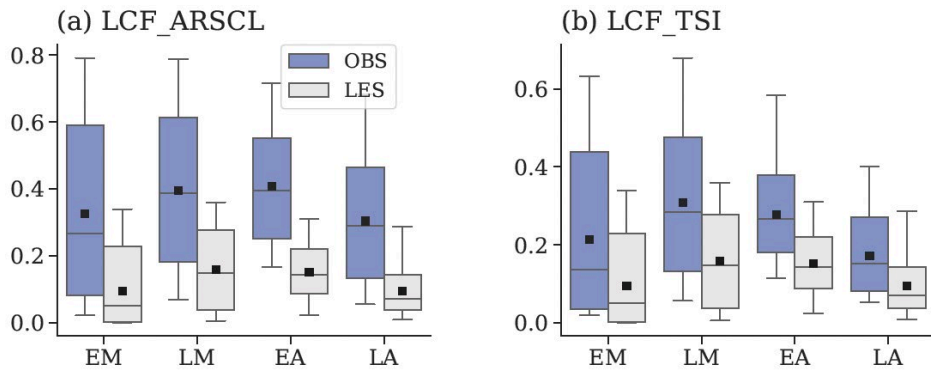
57  
58



59  
60  
61  
62  
63  
64  
65  
66  
67  
68

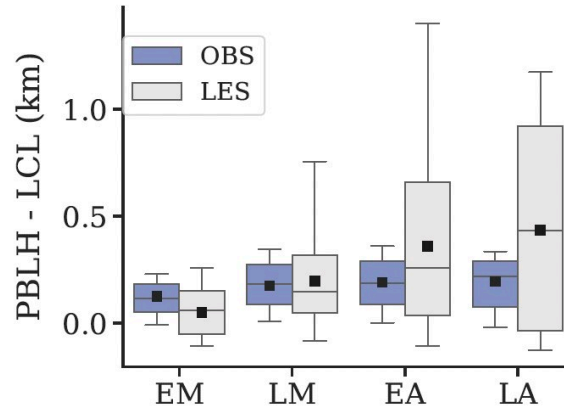
**Figure S4.** Time series of sensible heat fluxes (SHF) averaged for the 77 case days from observations (dashed curves) and LES runs (solid curves).

69



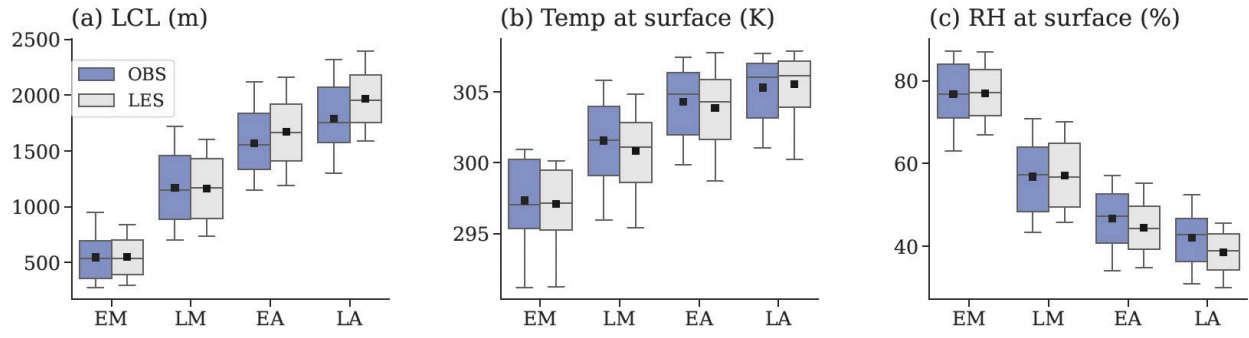
70  
71  
72  
73  
74  
75  
76

**Figure S5.** Same as Figure 2c but for comparisons between ARM Active Remote Sensing of Clouds (ARSCL)-derived low-cloud fraction (LCF) and Total Sky Imager (TSI)-derived LCF.



77  
78  
79  
80  
81  
82  
83

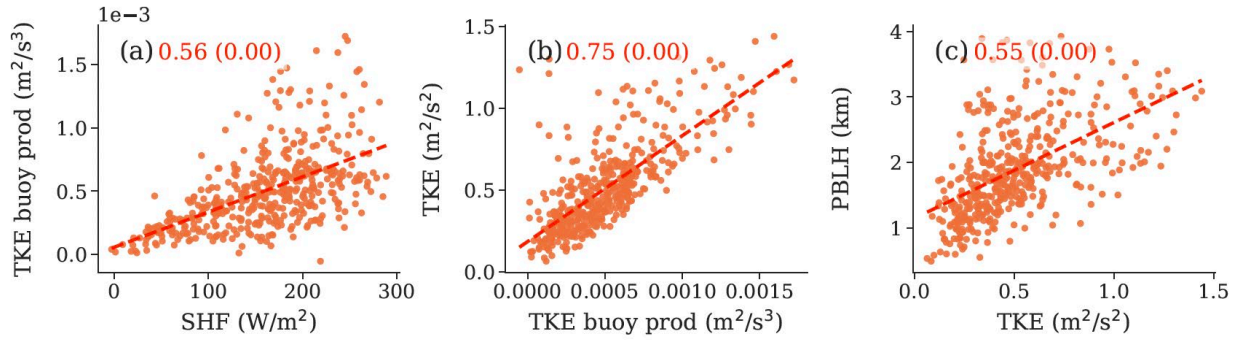
**Figure S6.** Same as Figure 2c but for planetary boundary-layer height (PBLH) minus lifted condensation level (LCL), which represents the tendency of the shallow convective trigger. The larger the value is, the more easily shallow convection is triggered.



84  
85  
86  
87  
88  
89

**Figure S7.** Same as Figure 2c but for lifted condensation level (LCL), near-surface temperature, and near-surface relative humidity (RH).





90  
 91  
 92  
 93  
 94  
 95  
 96  
 97  
 98  
 99  
 100

**Figure S8.** Scatter plots of (a) the turbulent kinetic energy (TKE) tendency due to buoyancy production versus sensible heat fluxes (SHF), (b) TKE versus the TKE tendency due to buoyancy production, and (c) planetary boundary-layer height (PBLH) versus the TKE, from 1000 LT to 1700 LT. Note that the TKE and its tendency shown are both the column-mean values. The dashed lines are best-fit lines from linear regression. Unbracketed numbers are the correlation coefficients between the two variables in each panel, with p-values shown in brackets.